Polymer Chemistry

ROYAL SOCIETY OF CHEMISTRY

PAPER

View Article Online
View Journal | View Issue

Cite this: *Polym. Chem.*, 2025, **16**, 2378

Deep eutectic ion-conductive hybrids produced by combining hydroxyl-functionalized silsesquioxane and mono-/difunctional hydrogen bond acceptors†

Tomohito Inoue, Sota Saito, Akihiro Nishioka and Hideharu Mori *

Received 26th February 2025,
Accepted 10th April 2025

DOI: 10.1039/d5py00192g

rsc.li/polymers

The use of ion-conductive organic–inorganic hybrids with high ionic conductivity, suitable flexibility/viscosity, and good thermal and mechanical properties is a promising approach for the development of next-generation, safer solid-state electrolytes. In this study, a series of new deep eutectic silsesquioxane (SQ) hybrids (DESQs) were developed by simply mixing hydroxyl-functionalized SQ acting as a polyol-type hydrogen bond donor (HBD) with imidazolium- and ammonium-based organic salts acting as hydrogen bond acceptors (HBAs) in the presence of a small amount of difunctional HBAs without the use of volatile organic solvents. The use of cross-linkable HBAs results in improved thermal stability and tunable flexibility (glass transition temperature and viscosity). The combination of hydroxyl-functionalized SQs and imidazolium salt-based mono-/difunctional HBAs afforded hybrids with hydrogen bond networks, showing a suitable balance between thermal properties and high ionic conductivity (4.17×10^{-4} S cm^{-1} at 25 °C), while maintaining reasonable viscosity (5.62×10^{6} mPa S at 25 °C). The ionic conductivity can be improved by adding a lithium salt, allowing for an efficient approach for obtaining safer, greener, and cost-effective electrolytes with good ionic conductivity.

Introduction

Deep eutectics, frequently called deep eutectic solvents (DESs), have been intensively investigated as promising environmentally friendly compounds that contribute to green chemistry and a sustainable society because of their attractive properties, such as high thermal stability, non-flammability, negligible vapor pressure, low toxicity, and low cost.[1–4] Deep eutectics consist of two or more solid substances and therefore are substantially distinct from ionic liquids, which are single molecules consisting of a single cation and a single anion in the molecule, even though some properties of deep eutectics (*e.g.*, non-flammability and negligible vapor pressure) are similar to those of ionic liquids. In deep eutectics, the interaction between a hydrogen bond acceptor (HBA, *e.g.*, organic salts) and a hydrogen bond donor (HBD, *e.g.*, urea derivatives) affords a eutectic mixture with a melting point remarkably lower than those of the individual original compounds due to self-association. Their potential applications have been extended from basic research (*e.g.*, organic synthesis,[5] dissociation/extraction,[2] catalysis,[6] and metal processing[3,7]) to advanced materials (*e.g.*, nanomaterials,[8,9] polymers,[7,10,11] soft materials,[12] bioinspired inorganic–organic materials,[13] and energy-related materials[14]). In particular, the preorganized nature of DESs allows them to serve as inorganic stabilizers and soft templates for the production of hybrids with hierarchical structures ranging from the atomic to the macroscopic level, which can provide modern bioinspired materials with sophisticated features.[13]

Deep eutectic electrolytes (DEEs) have been the focus of recent developments in this field and are eutectics that can be used as electrolytes in electrochemical devices such as lithium batteries.[15–21] Distinct from flammable organic electrolytes, DEEs consisting of a solid salt (HBA) and a solid HBD offer the potential advantages of improved safety and reduced risk of volatilization and ignition. Another attractive feature of DEEs is their ability to achieve relatively high Li^+ transfer numbers owing to the presence of a single cation species,[16,17] which is essentially distinct from ionic liquids frequently used as non-flammable electrolytes. Research on DEEs is a dynamically developing field, and a wide variety of HBD/HBA combinations have been continuously introduced into DEEs, offering greater versatility, higher ion conductivity, wider electrochemical windows, and greater safety and higher robustness. A

Department of Organic Materials Science, Graduate School of Organic Materials Science, Yamagata University, 4-3-16, Jonan, Yonezawa City, Yamagata Prefecture 992-8510, Japan. E-mail: h.mori@yz.yamagata-u.ac.jp

† Electronic supplementary information (ESI) available. See DOI: https://doi.org/10.1039/d5py00192g

variety of pioneering studies have been recently reported in this field, *e.g.*, potential and advantageous aspects of DEEs and DESs for low-temperature metal-ion batteries,[22] electrochemical energy storage and conversion,[23] and effectiveness of computational methods to accelerate the discovery and material design of novel DES-based materials.[24]

Solid-state electrolytes, such as polymeric materials and gels consisting of DEE units, have been developed as safer, greener, and cost-effective electrolytes.[12,25–29] Despite the wide variety of research studies on solid-state electrolytes, development of new ion-conductive organic–inorganic hybrids based on a novel approach is required to overcome the inherent tradeoff between ionic conductivity and solidification. For instance, solid composite electrolytes consisting of inorganic silica surrounding a lithium-ion-conducting DEE have been developed.[30] Another intriguing example of the efficient employment of DESs involves the synthesis of siloxane-based self-healing gel electrolytes for quasi-solid-state lithium metal batteries.[31] Silsesquioxane (SQ), a silicon-containing compound characterized by a silicon/oxygen ratio of 1.5, has been employed as an inorganic core with an organic shell of quaternary-ammonium/urea derivative DEEs.[32] These organic–inorganic hybrids possess a unique combination of various advantages of DEEs and inorganic components, *e.g.*, silica (SiO_2) and SQs $(R\text{-}SiO_{1.5})_n$ (n = even number). Their low cost, suppressed flammability, and a wide variety of possible HBD/HBA combinations make DEE-based hybrids excellent candidates for the discovery of novel hybrids with favorable performance that are suitable for industrial-scale utilization. In addition, ionic liquid-based SQs have been developed to produce ion-conductive organic–inorganic hybrids as solid-state electrolytes for future battery applications.[33–37]

In this study, a simple, efficient, and volatile organic solvent-free green method for creating ion-conductive organic–inorganic DESQ hybrids by combining deep eutectics and SQ nanoparticles was demonstrated. Ion-conductive organic–inorganic hybrids were prepared by mixing hydroxyl-functionalized SQ nanoparticles as HBDs, quaternary ammonium salt- or imidazolium salt-based HBAs, and difunctional cross-linkable HBAs, as shown in Fig. 1. Among various categories of DESs defined previously by Abbott *et al.*,[3,38] much attention has been paid to type III DESs consisting of a quaternary ammonium salt as the HBA and an organic molecule such as amide, carboxylic acid, and polyol (*e.g.*, ethylene glycol, glycerol, and xylitol) compounds as the HBD, owing to their low melting points, composition flexibility, and potential applications.[1,13,39] In this study, hydroxyl-functionalized SQ nanoparticles (an average particle size of approximately 3 nm) prepared by the reaction of (3-aminopropyl)triethoxysilane and glycidol followed by hydrolytic condensation with more than 50 hydroxyl groups on the SQ surface[40,41] were selected as polyol-type HBDs. The formation of DESQ hybrids is based on noncovalent interactions between multifunctional hydroxyl groups (multi-HBD units) in the organic chains covalently linked to SQ and the monofunctional HBA in the presence of a small portion of the difunctional HBA. Three monofunctional HBAs, namely tetrabutylammonium chloride (TBACl), choline chloride (ChCl), and 1-ethyl-3-methylimidazolium bromide (EMIBr), were selected and can be regarded as quaternary ammonium salt- and imidazolium salt-based HBAs. Difunctional cations ($(MITFSI)_2C_4O$ and $(MITFSI)_2C_2$) were used as cross-linkable HBAs. The potential advantages of DESQ hybrids include tunable solidity/viscosity, hardness/flexibility, and ionic conductivity *via* the HBD/HBA balance and the exploitation of numerous possible HBD/HBA combinations. To simultaneously achieve high ionic conductivity, suitable viscosity, and thermal properties, an appropriate balance between the HBDs on SQ/monofunctional HBA/difunctional HBA is crucial. Increasing the difunctional HBA content may lead to an increase in the cross-linking density, improving the thermal and mechanical properties, but it may also reduce the flexibility and therefore ionic conductivity. Hence, a good balance between HBD/HBA/cross-linkable HBA and their suitable combination is required to achieve the

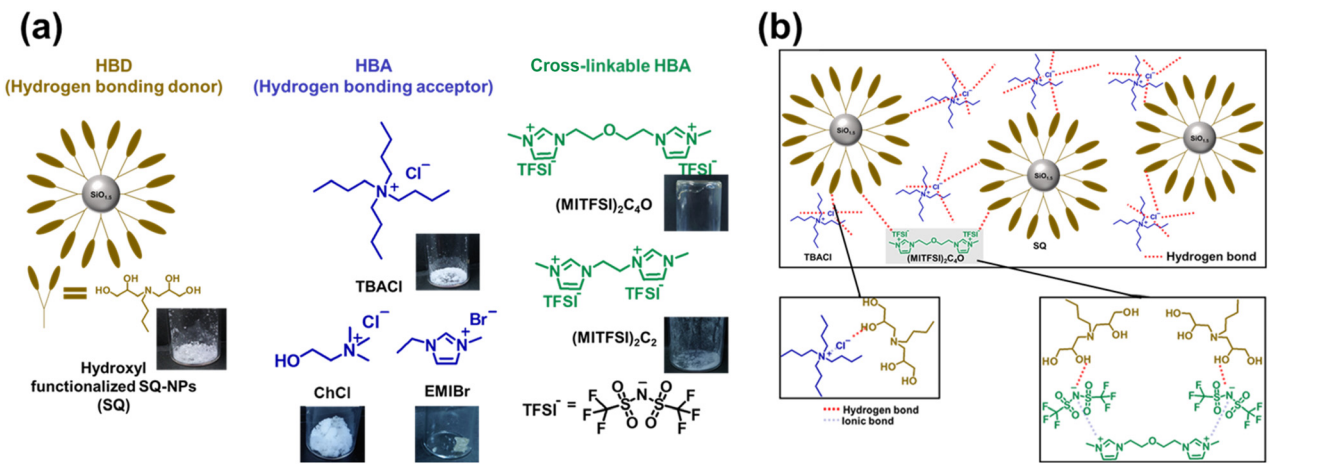

Fig. 1 (a) Structures of the HBD (hydroxyl-functionalized SQ nanoparticles), HBAs (TBACl, ChCl, and EMIBr), and cross-linkable HBAs ($(MITFSI)_2C_4O$ and $(MITFSI)_2C_2$) used in this study. (b) Postulated cross-linking structures of DESQ hybrids formed through hydrogen bonds.

desired deep eutectic effects and high ionic conductivity. The fabrication of inorganic SQs with designed DEE structures consisting of a suitable HBD/HBA combination is a promising green approach for basic research on DEE-based organic–inorganic hybrids and future industrial applications.

Results and discussion

Two-component DESQ hybrids

As a polyol-type HBD, hydroxyl-functionalized SQ was prepared by the reaction of (3-aminopropyl)triethoxysilane and glycidol, followed by hydrolytic condensation,[40,41] and has the basic unit of (R-$SiO_{1.5}$) with a molecular weight of 258.3, where R corresponds to an organic chain with four hydroxyl groups originating from glycidol. Each SQ was reported to contain approximately 14.6 Si atoms (12–18 Si atoms), suggesting the presence of 58 hydroxyl groups on average.[40,41] A quaternary ammonium salt-based HBA (TBACl, T_m = 70 °C) and an imidazolium salt-based HBA (EMIBr, T_m = 74 °C) were used as representative monofunctional HBAs (Table S1 and Fig. S2 and S3†). Two-component DESQs were prepared through the reaction of hydroxyl groups covalently linked to SQ with two different HBAs (TBACl and EMIBr) at different feed ratios ([R-$SiO_{1.5}$]/[HBA] = 100/50, 100/100, and 100/200, abbreviated as SQ/HBA (x/y)), corresponding to [OH group]/[HBA] = 8/1, 4/1, and 2/1, respectively. As shown in Table 1, a solid-to-liquid transformation was observed after mixing the hydroxyl-functionalized SQ with TBACl and EMIBr at 60 °C for 24 h, implying the successful formation of viscous DESQ hybrids. In both cases, the viscous hybrids were maintained at room temperature without solidification and were employed directly for further investigation. Under these conditions, the hydrogen bonds between the hydroxyl groups on SQ and the monofunctional HBA (TBACl or EMIBr) were sufficiently strong to achieve a eutectic effect, lowering the melting point, while the interaction was weak enough to prevent the formation of cocrystal structures. Hydrogen bonds between the HBA and the HBD have been reported to weaken the inherent electrostatic attraction between the cation and the anion in the pristine HBA[13,42] (TBACl or EMIBr in the present system). When the hydroxyl-functionalized SQ was reacted with tetrabutylammonium bromide (100/50, 100/100, and 100/200) under the same conditions, the solid components remained even after mixing at 60 °C for 24 h (Table S2†), suggesting the importance of a suitable selection of a counter anion.

Nuclear magnetic resonance (NMR) analysis was employed to characterize the two-component DESQ hybrids. The ^{1}H NMR spectrum of SQ/TBACl (100/200) in D_2O (Fig. S5†) exhibited four sharp peaks at 3.14, 1.56, 0.88, and 1.30 ppm, corresponding to the butyl group in TBACl, in addition to broad resonances at approximately 0.4–0.7, 1.4–1.8, 2.4–2.9, and 3.2–4.0 ppm attributed to the methylene and methine units of the organic chain linked covalently to the SQ core. Similar

Table 1 Preparation and thermal properties of two-component DESQ hybrids by the reaction of SQ and HBAs[a]

Two-component hybrid	T_{d5}[b] (°C)	T_g[c] (°C)	Residual weight[d] (%)	Appearance 0 h	Appearance 24 h
R-$SiO_{1.5}$/TBACl (100/200)	196	−30.2	14.1		
(100/100)	198	−12.5	14.7		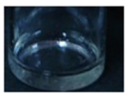
(100/50)	214	−12.4	19.8		
R-$SiO_{1.5}$/EMIBr (100/200)	258	17.2	20.7		
(100/100)	257	−17.6	22.6		
(100/50)	257	−14.0	15.9		

[a] Two-component DESQ hybrids were prepared by mixing the hydroxyl-functionalized SQ with tetrabutylammonium chloride (TBACl) and 1-ethyl-3-methylimidazolium bromide (EMIBr) at 60 °C for 24 h. [b] Temperature for 5 wt% weight loss under nitrogen. [c] Determined by DSC. [d] Residual weight of the sample heated at 10 °C min^{-1} until 700 °C in TGA under nitrogen.

broad peaks attributed to the restricted motion of the organic chain attached to the SQ core were also observed in the ^{1}H NMR spectrum of SQ/EMIBr (100/200) in D_2O, with two sharp peaks at 7.3 and 8.6 ppm corresponding to the imidazolium unit (Fig. S6†).

TGA and DSC measurements were conducted on the two-component DESQs prepared using the two HBAs (TBACl and EMIBr) at different feed ratios. As shown in Fig. 2a, the TGA results for the SQ/TBACl (100/100 and 100/200) hybrids showed sharp decomposition over the 180–240 °C range, which is most likely due to the decomposition of the HBA (TBACl in this case), and the subsequent gradual decomposition over the 240–500 °C range, which is attributed to the decomposition of pristine SQ. The SQ/TBACl (100/50) hybrid showed intermediate decomposition behavior between those of SQ/TBACl (100/100) and pristine SQ (Table S3†). The 5 wt% weight loss (T_{d5}) values of the two-component hybrids were 196, 198, and 214 °C for the SQ/TBACl (100/200, 100/100, and 100/50) hybrids, respectively, substantially lower than that of pristine SQ (T_{d5} = 229 °C). The char yields for the SQ/TBACl hybrids were between 14.1% and 19.8%, lower than that of SQ (29%), implying that the incorporation of an organic salt (TBACl) resulted in a slight decrease in the thermal stability. Two-component SQ/EMIBr (100/50, 100/100, and 100/200) hybrids showed similar decomposition behaviors, as shown in Fig. 2b, while they exhibited higher thermal stability (T_{d5} = 257–258 °C) compared to that of SQ/TBACl hybrids, which is most likely due to the higher thermal stability of EMIBr (235 °C) compared to that of TBACl (187 °C). The glass transition temperature (T_g) of the SQ/TBACl hybrids increased from −30.2 °C to −12.4 °C with decreasing HBA content, while the T_g values of the SQ/EMBr (100/200 and 100/50) hybrids were 17.2 °C and −14.0 °C, respectively.

Viscoelasticity measurements of the SQ/TBACl and SQ/EMIBr two-component DESQs (100/200 in both cases) were conducted using rheological temperature sweeping. When the temperature increased from 25 °C to 60 °C, the storage (G') and loss (G'') moduli of the SQ/EMIBr hybrid decreased gradually, showing a cross-over temperature T_c, where G' (T_c) = G'' (T_c), of approximately 29.1 °C (Fig. 2d). The SQ/EMIBr hybrid exhibited elastic behavior at temperatures lower than T_c ($G' > G''$) and viscous behavior at higher temperatures ($G' < G''$). In contrast, the SQ/TBACl hybrid was found to be in a heterogeneous state between 25 °C and 50 °C and exhibited viscous behavior ($G' < G''$) at higher temperatures in the range of 50–70 °C (Fig. 2c). The ionic conductivities of two-component DESQs prepared using two HBAs (TBACl and EMIBr) at different feed ratios were evaluated using electrochemical impedance spectroscopy. The ionic conductivity of SQ/EMIBr (100/200) was found to be the highest (4.91×10^{-4}, 8.66×10^{-4}, 1.21×10^{-3}, and 4.35×10^{-3} S cm^{-1} at 25, 45, 55, and 90 °C, respectively), which is most likely due to the planar structure of the imidazole ring. The relatively low ionic conductivity of SQ/TBACl is probably attributed to the steric hindrance caused by the free rotation of the four butyl groups.

Three-component DESQ hybrids

Two imidazolium-based cross-linkable HBAs were prepared by reacting 1-methylimidazole with bis(2-bromoethyl)ether and 1,2-dibromoethane, followed by reaction with LiTFSI, as reported previously.[43,44] When the SQ was reacted with TBACl in the presence of $(MITFSI)_2C_4O$ at [R-$SiO_{1.5}$]:[TBACl]:[$(MITFSI)_2C_4O$] = 100:200:1, 5, and 10, the white solid mixture turned into a transparent viscous liquid at 60 °C for 24 h (Table 2). These combinations have been abbreviated as SQ/HBA/crosslinker ($x/y/z$), where HBA/crosslinker represents the HBA (TBACl or EMIBr) and the crosslinker ($(MITFSI)_2C_4O$ or $(MITFSI)_2C_2$), respectively, and $x/y/z$ corresponds to the feed ratio (Table S4†). The resulting three-component SQ/TBACl/$(MITFSI)_2C_4O$ (100/200/1) was kept in the eutectic viscous state that showed improved thermal stability (T_{d5} = 233 °C) compared to that of the two-component SQ/TBACl (100/200) hybrid (T_{d5} = 196 °C). DSC measurements of the SQ/TBACl/$(MITFSI)_2C_4O$ (100/200/1) hybrid revealed that the T_g value was below room temperature (T_g = 0.0 °C), which is between the T_g values for the two-component SQ/TBACl (100/200) hybrid (−30.2 °C) and the SQ/EMIBr (17.2 °C) hybrid. The addition of the cross-linkable HBA led to a substantial increase in T_{d5} and T_g, indicating an improvement in the thermal properties of the SQ/TBACl hybrid (Fig. S8 and S11 and Table S5†). Similar degradation behaviors were observed in the TGA traces of both the ammonium- and imidazolium salt-based hybrids (SQ/EMIBr/$(MITFSI)_2C_4O$ and $(MITFSI)_2C_2$). For the SQ/EMIBr hybrids, no remarkable increase in T_{d5} was observed, whereas T_g increased in all combinations with the incorporation of the cross-linkable HBA (Fig. S9, S10, S12, and S13 and Table S5†),

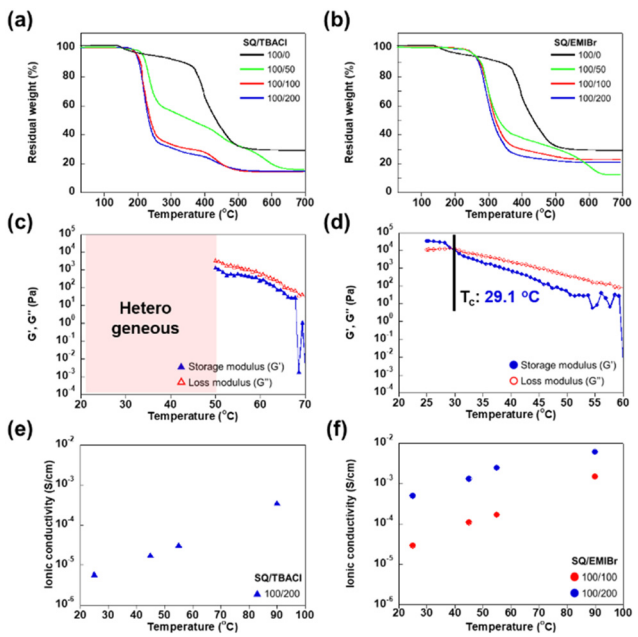

Fig. 2 (a and b) TGA curves, (c and d) storage (G') and loss (G'') moduli against temperature, and (e and f) temperature-dependent ionic conductivities of (a, c and e) SQ/TBACl and (b, d and f) SQ/EMIBr hybrids.

Table 2 Preparation and thermal properties of three-component DESQ hybrids by the reaction of SQ, HBAs, and cross-linkable HBAs

Three-component hybrid	T_{d5}[a] (°C)	T_g[b] (°C)	Residual weight[c] (%)	Appearance 0 h	Appearance 24 h
$RSiO_{1.5}$/TBACl/$(MITFSI_2)C_4O$ (100/200/1)	233	0.0	30.6		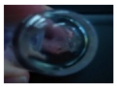
(100/200/5)	188	−38.4	7.32		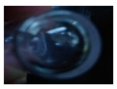
(100/200/10)	189	−37.6	9.97		
R-$SiO_{1.5}$/EMIBr/$(MITFSI_2)C_4O$ (100/200/1)	252	38.1	16.3		
(100/200/5)	—	—	—		
(100/200/10)	—	—	—		
R-$SiO_{1.5}$/EMIBr/$(MITFSI_2)C_2$ (100/200/1)	255	32.6	17.7	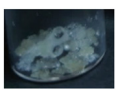	
(100/200/5)	248	3.1	15.3		
(100/200/10)	254	2.4	14.7		

[a] Temperature for 5 wt% weight loss under nitrogen. [b] Determined by DSC. [c] Residual weight of the sample heated at 10 °C min^{-1} until 700 °C in TGA under nitrogen.

implying the formation of cross-linked structures with improved thermal properties originating from the cross-linkable HBA.

The FT-IR spectra of the three-component SQ/TBACl/$(MITFSI)_2C_4O$ (100/200/1) and two-component SQ/TBACl (100/200) hybrids showed the preserved OH functional group as indicated by the broad absorption from 3000 to 3800 cm^{-1} with the peak located at approximately 3397 and 3349 cm^{-1}, respectively (Fig. S14†). These absorption peaks are slightly shifted from the peak of the pristine hydroxyl-functionalized SQ (3369 cm^{-1}), most likely due to the presence of hydrogen bonding. Additionally, sharp peaks were observed between 2944 and 2873 cm^{-1}, attributed to the C–H stretching vibration in the alkyl chain, and at 1473 cm^{-1}, corresponding to the C–H bending vibrations in the TBACl unit. In both hybrids, a weak band at approximately 1124–1039 cm^{-1} was detected, which is ascribed to Si–O–Si stretching originating from the SQ-based hybrids. Similar characteristic peaks were also detected in the FT-IR spectra of the three-component SQ/EMIBr hybrids (Fig. S14†).

The temperature-dependent complex viscosity ($|\eta^*|$) was measured for the two-component and three-component hybrids using a rotational rheometer. As shown in Fig. 3a–c, the incorporation of a small amount of the cross-linker ($(MITFSI)_2C_4O$ or $(MITFSI)_2C_2$) had a remarkable impact on the rheological properties of the SQ/EMIBr and SQ/TBACl hybrids. For both imidazolium- and ammonium-based hybrids, three-component hybrids with the cross-linker showed higher $|\eta^*|$ values than two-component hybrids. Generally, high viscosities of DESs originate from the hydrogen bond networks formed between the HBD/HBA constituent compounds, in addition to other interactions (*e.g.*, ionic and van der Waals interactions), affecting the mobility and diffusion of ions and molecules.[13] Incorporation of the cross-linker HBA leads to an increase in cross-linking density and therefore the viscosity of the DESQ hybrids. In all cases, the values of $|\eta^*|$ of the two- and three-component hybrids decreased with increasing temperature, which is consistent with a general tendency of DESs, showing an exponential decrease in the viscosity with increasing temperature.[13]

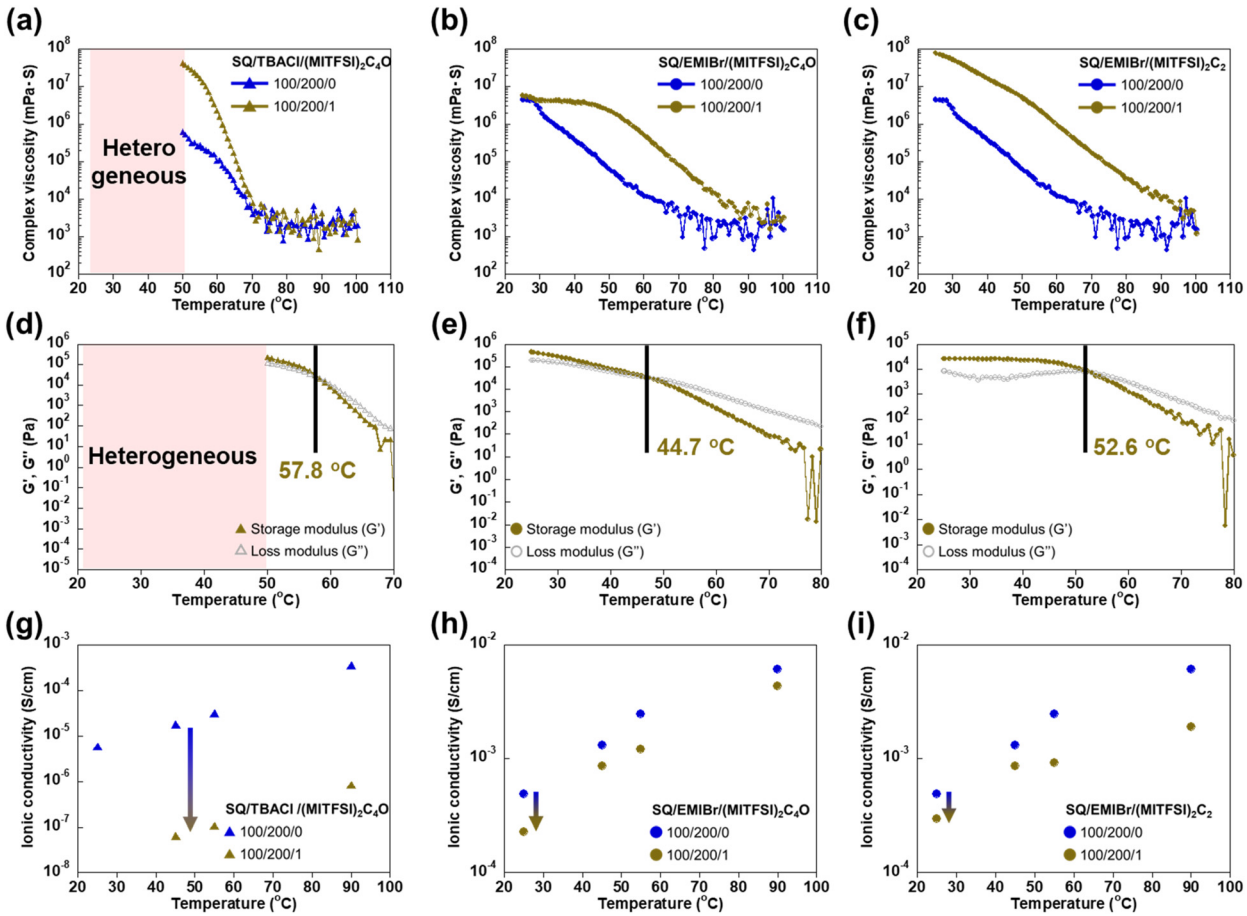

Fig. 3 (a–c) Complex viscosities, (d–f) storage (G') and loss (G'') moduli against temperature, and (g–i) temperature-dependent ionic conductivities of three-component (100/200/1) and two-component (100/200) hybrids. (a, d and g) SQ/TBACl/$(MITFSI)_2C_4O$, (b, e and h) SQ/EMIBr/$(MITFSI)_2C_4O$, and (c, f and i) SQ/EMIBr/$(MITFSI)_2C_2$.

Nevertheless, the temperature dependence of the viscosity ($|\eta^*|$) was affected by the cross-linker ($(MITFSI)_2C_4O$ and $(MITFSI)_2C_2$) and HBA (imidazolium- and ammonium-based hybrids). As shown in Fig. 3d–f, the measured T_c values were 57.8, 44.7, and 52.6 °C for SQ/TBACl/$(MITFSI)_2C_4O$, SQ/EMIBr/$(MITFSI)_2C_4O$, and SQ/EMIBr/$(MITFSI)_2C_2$ (100/200/1 for all cases). These values are higher than those of the two-component systems, suggesting that the range of elastic behaviors can be extended by the addition of the cross-linkable HBA.

The ionic conductivities of the three-component hybrids (100/200/1 in all cases) were evaluated under ambient conditions. As shown in Fig. 3g–i, both SQ/EMIBr/$(MITFSI)_2C_4O$ and SQ/EMIBr/$(MITFSI)_2C_2$ exhibit higher ionic conductivity (9.23×10^{-4}–2.47×10^{-3} S cm^{-1} at 55 °C) than SQ/TBACl/$(MITFSI)_2C_4O$ (1.07×10^{-7} S cm^{-1} at 55 °C). In all cases, the addition of the cross-linkable HBA led to a decrease in the ionic conductivity, most likely due to the restriction of chain mobility by cross-linking and the decrease of ion mobility. However, a limited effect of the cross-linker on the decrease in the ionic conductivity was observed for the imidazolium salt-based hybrids (SQ/EMIBr/$(MITFSI)_2C_4O$ and $(MITFSI)_2C_2$). In contrast, the ionic conductivity of SQ/TBACl/$(MITFSI)_2C_4O$ was more than two orders of magnitude lower than that of the two-component SQ/TBACl (100/200) hybrid, suggesting a remarkable effect of the crosslinker on the quaternary ammonium salt-based hybrids. The activation energy for the ionic conductivity of SQ/EMIBr (100/200) calculated from the Arrhenius plot (Fig. S15†) was 35.0 kJ mol^{-1}, which was substantially lower than those (54–58 kJ mol^{-1}) of SQ/TBACl (100/200) and SQ/EMIBr (100/100). No significant effect of the cross-linker on the activation energy was observed for the SQ/TBACl hybrids (55.5 kJ mol^{-1} for SQ/TBACl/$(MITFSI)_2C_4O$ and 57.3 kJ mol^{-1} for SQ/TBACl (100/200), Fig. S16 and Table S6†). The addition of $(MITFSI)_2C_4O$ to the SQ/EMIBr (100/200) hybrid (activation energy = 35.0 kJ mol^{-1}) led to a slight increase in the activation energy (40.1 kJ mol^{-1}), while a slight decrease in the activation energy was observed upon the addition of $(MITFSI)_2C_2$ (27.0 kJ mol^{-1}). Nevertheless, the imidazolium-salt-based three-component hybrids (SQ/EMIBr) with cross-linkers ($(MITFSI)_2C_4O$ and $(MITFSI)_2C_2$) exhibited improved thermal stability with wider elastic states, owing to the enhanced degree of cross-linking, while maintaining ionic conductivity, most likely due to the planar structure of the imidazole ring. The SQ/EMIBr/$(MITFSI)_2C_4O$ combination exhibited the best balance between

the ionic conductivity and the thermal and mechanical properties.

Different tendencies in the preparation and properties of the ChCl-based hybrids were observed. Compared to TBACl and EMIBr, ChCl, which is a representative HBA for DES formation, has a higher melting point (T_m = 302 °C). When ChCl was mixed with SQ as a binary system, even though a drop in the melting point occurred, SQ/ChCl showed no solid-to-liquid transformation. In contrast, solid-to-liquid transformation was observed for the preparation at an [R-$SiO_{1.5}$]/[ChCl]/[$(MITFSI)_2C_4O$] of 100/50/1 when the eutectic mixture was generated using a lower feed ratio of ChCl compared to other HBAs at higher temperature for a longer mixing time (80 °C, 48 h, Fig. 4a). In the ChCl-based hybrids, a small portion of $(MITFSI)_2C_4O$ may have acted as a plasticizer, and the presence of a hydroxyl group in ChCl may have affected the HBD/HBA ratios, affording a homogeneous DESQ hybrid. TGA measurements of SQ/ChCl/$(MITFSI)_2C_4O$ (100/50/1) demonstrated its good thermal stability (T_{d5} = 244 °C, Fig. 4b), which is comparable to those of the TBACl- and EMIBr-based three-component hybrids and is intermediate between the T_{d5} values of ChCl (280 °C) and SQ (229 °C). DSC measurements revealed a T_g value below 0 °C (−24.9 °C, Fig. 4c). The FT-IR spectra showed peaks derived from the hydroxyl groups of SQ and ChCl (SQ: 3257 cm^{-1} and ChCl: 3369 cm^{-1}), which shifted to 3361 and 3367 cm^{-1}, respectively, in the three-component hybrid (Fig. 4d), confirming the formation of hydrogen bonds. In addition, peaks originating from SQ and ChCl were detected in the three-component hybrids. The ionic conductivity of the ChCl-based hybrid was 2.20×10^{-7} S cm^{-1} at room temperature (Fig. 4e), which is intermediate between the values for the TBACl- and EMIBr-based three-component hybrids. The free rotation of the three methyl groups around the ammonium ion in ChCl may contribute to steric hindrance, resulting in a lower ionic conductivity than that of the EMIBr-based hybrid. In addition, the hydroxyl group in ChCl can act as a structural trap for the cation and reduce its degrees of freedom, which may be the origin of the lower ionic conductivity. In contrast, the lower steric hindrance of ChCl may contribute to better ionic conductivity compared to that of the bulky TBACl-based hybrid.

Three quaternary ammonium salt-based cross-linkable HBAs were also prepared from *N*,*N*,*N*′,*N*′-tetramethylethylenediamine and bis(2-dimethylaminoethyl)ether combined with iodomethane, followed by reaction with LiTFSI (Fig. S1†). These cross-linkable HBAs were used to produce DESQ hybrids, whereas the solid components partially prevented the formation of homogeneous viscous products, implying a limited eutectic effect (Table S4†). In other words, two imidazolium-based cross-linkable HBAs, ($(MITFSI)_2C_4O$ and $(MITFSI)_2C_2$), used mainly in this study, were effective in achieving a sufficient eutectic effect and homogeneous DESQ

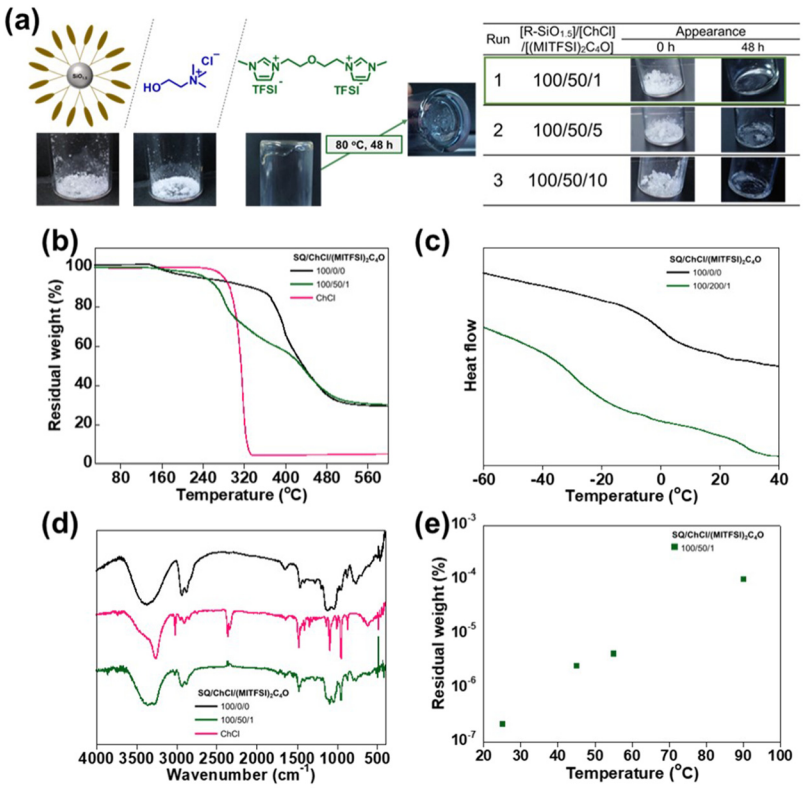

Fig. 4 (a) Photographs, reaction conditions, and results, (b) TGA curves, (c) DSC curves, and (d) FT-IR spectra of SQ and three-component DESQ ([R-$SiO_{1.5}$]/[ChCl]/[$(MITFSI)_2C_4O$] = 100/200/1). (e) Temperature-dependent ionic conductivity of SQ/ChCl/$(MITFSI)_2C_4O$ (100/200/1).

hybrids. From the structural viewpoint, $(MITFSI)_2C_4O$ has a longer alkyl spacer with an ether unit, while $(MITFSI)_2C_2$ has an ethylene spacer between the two imidazolium units. The different spacers may contribute to the difference in the cross-linking density and spatial distance between SQ nanoparticles in the three-component hybrids. The incorporation of a small amount of the imidazolium-based cross-linkable HBA efficiently enhanced the thermal properties, but it led to a decrease in the flexibility and therefore ionic conductivity. These results suggest that the mono- and difunctional HBAs and the HBD/monofunctional HBA/difunctional HBA composition must be properly selected to obtain homogeneous viscous hybrids with high ionic conductivity, suitable viscosity, and thermal properties under the assumed conditions.

Three-component DESQ hybrids with a lithium salt

The effects of the addition of a Li salt to the three-component hybrids (SQ/TBACl/$(MITFSI)_2C_4O$, SQ/EMIBr/$(MITFSI)_2C_4O$, and SQ/EMIBr/$(MITFSI)_2C_2$) on their thermal and ion-conductive properties were evaluated. A representative Li salt (LiTFSI) was selected to confirm its ability to produce homogeneous hybrids with improved ionic conductivity and thermal properties. Predetermined amounts of LiTFSI were mixed with a mixture of SQ, HBA (TBACl or EMIBr), and difunctional HBA to obtain three-component DESQ hybrids with increasing lithium salt concentrations (LiTFSI: 10, 20, 30 and 40 wt%, as shown in Table S7†). The SQ : HBA : difunctional HBA ratio was kept constant at 100 : 200 : 1 based on the results obtained in the previous section. When 10 wt% LiTFSI was mixed with the three-component systems, homogeneous hybrids were obtained, regardless of the SQ/HBA/cross-linker combination. However, undissolved LiTFSI remained as a white solid in the heterogeneous hybrids when the Li-salt content increased to 20–40 wt% (Fig. S17†). Hence, three-component hybrids (SQ/HBA/cross-linker) with 10 wt% LiTFSI were employed for further evaluation. As shown in Fig. 5a–c, the thermal stability of SQ/TBACl/$(MITFSI)_2C_4O$ decreased significantly upon the addition of 10 wt% LiTFSI (T_{d5} = 195 °C and 233 °C for hybrids with and without LiTFSI, respectively), while no substantial effect due to the Li salt was observed on the thermal stability of the imidazolium-based hybrids (SQ/EMIBr/$(MITFSI)_2C_4O$ and SQ/EMIBr/$(MITFSI)_2C_2$). The incorporation of LiTFSI into the three-component hybrids was confirmed by FT-IR measurement (Fig. 5d–f). The addition of the lithium salt (LiTFSI) improved the ionic conductivity in all cases, and this tendency was affected by the combination of the three

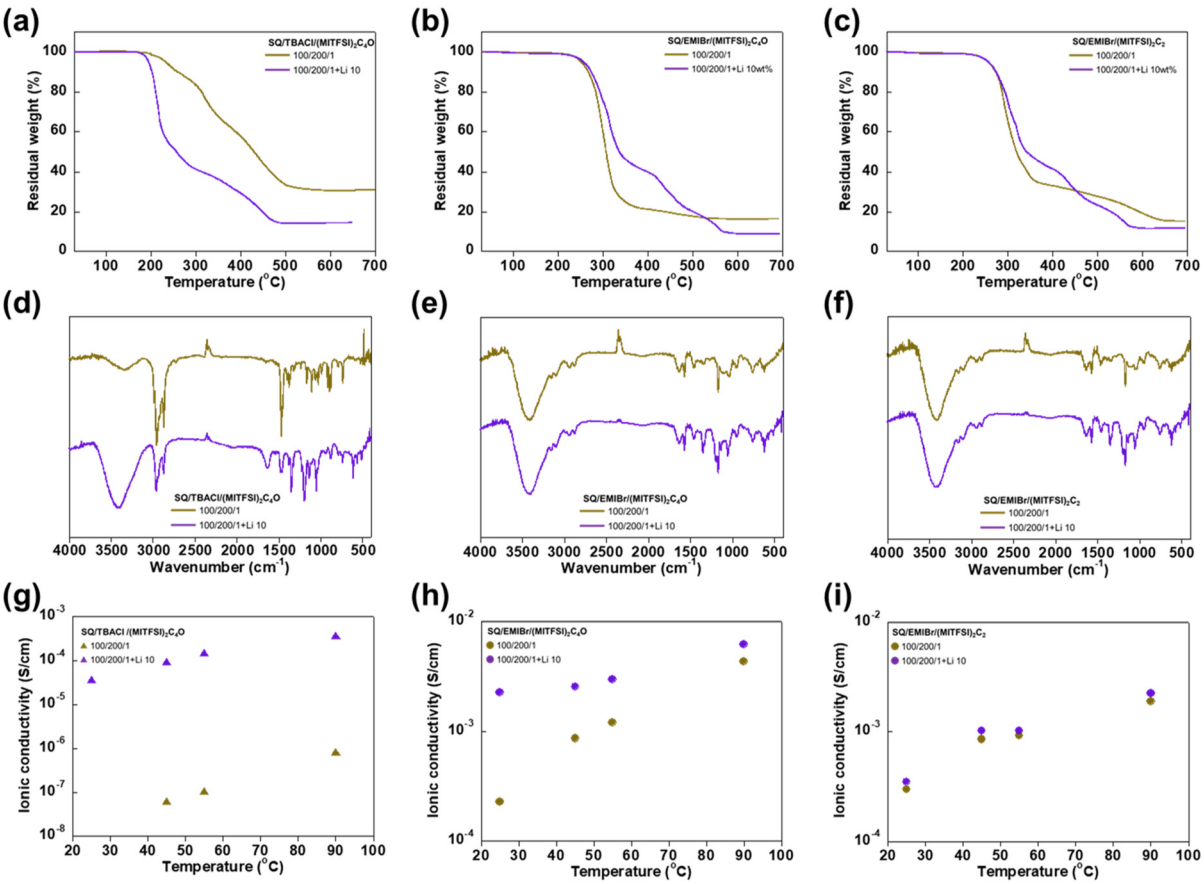

Fig. 5 (a–c) TGA curves, (d–f) FT-IR spectra, and (g–i) temperature-dependent ionic conductivities of two- and three-component Li hybrids. (a, d and g) SQ/TBACl/$(MITFSI)_2C_4O$–Li, (b, e and h) SQ/EMIBr/$(MITFSI)_2C_4O$–Li, and (c, fand i) SQ/EMIBr/$(MITFSI)_2C_2$–Li hybrids.

components (Fig. 5g–i). The ionic conductivities of the hybrids with 10 wt% LiTFSI were in the order of SQ/EMIBr/$(MITFSI)_2C_4O$ > SQ/EMIBr/$(MITFSI)_2C_2$ > SQ/TBACl/$(MITFSI)C_4O$, which was the same order as that of the three pristine hybrids. The ionic conductivities were 2.23×10^{-3}–3.77×10^{-5} S cm^{-1} at 25 °C (Table S8†), which were comparable to or higher than those of representative ionic-liquid-based SQs (10^{-4}–10^{-5} S cm^{-1} at 22–25 °C)[33–36] and composite polymer electrolytes (10^{-4}–10^{-7} S cm^{-1} at 24–30 °C).[45] These values were also comparable to those of representative DEEs (*e.g.*, 7.61×10^{-3} S cm^{-1} at 20 °C for ChCl/ethylene glycol (1/2)[23,46] and 0.76×10^{-3} S cm^{-1} at 25 °C for $LiNTf_2$/urea (1/3.6)).[18,23] The activation energies for the ionic conductivity of the hybrids with 10 wt% LiTFSI (24.6–35.5 kJ mol^{-1}) were substantially lower than those of the three-component hybrids (27.0–55.5 kJ mol^{-1}, Fig. S19 and Table S6†). The tendency is probably attributed to an increased movement of the organic units derived from increased viscosity at lower temperatures upon the addition of LiTFSI. A drastic decrease in T_{d5} due to the addition of LiTFSI was observed in the TBACl-based hybrids, whereas no significant change due to the addition of LiTFSI was observed for the EMIBr-based hybrids, which is most likely caused by the higher thermal stability of EMIBr (234.8 °C), compared to that of TBACl (186.9 °C). These T_{d5} values were higher than those of representative DEEs (*e.g.*, onset decomposition temperature = 111 °C for ChCl/ethylene glycol (1/2)[47] and 189 °C for ChCl/urea (1/2)[47] and T_{d5} = 178 °C for LiTFSI/urea (1/5)[19]), implying that the use of SQ nanoparticles improved the thermal stability.

To clarify the effect of the Li salt on the viscosity of the three-component DESQ hybrids, the temperature-dependent complex viscosity ($|\eta^*|$) was measured for the three-component Li hybrids (100/200/1 + LiTFSI 10 wt%). As shown in Fig. S20,† the addition of LiTFSI to the TBACl-based hybrid led to a remarkable decrease in the viscosity in a relatively low temperature range (<70 °C). Similarly, a decrease in the viscosity upon the addition of LiTFSI was observed for the EMIBr-based hybrids, while the effect was not significant, compared to that of the TBACl-based hybrid. The T_c values were 39.5 and 31.5 °C for the SQ/EMIBr/$(MITFSI)_2C_4O$–Li and SQ/EMIBr/$(MITFSI)_2C_2$–Li hybrids, respectively, which were lower than those of the corresponding EMIBr-based hybrids without LiTFSI (44.7 and 52.6 °C). These results suggest that the addition of LiTFSI to the three-component hybrids leads to a decrease in the viscosity and an increase in the temperature range, showing viscous behavior. Even if crosslinking leads to a substantial decrease in the ionic conductivity, the incorporation of a lithium salt (LiTFSI) may contribute to reducing the crosslink density, resulting in the simultaneous achievement of both high ionic conductivity and heat resistance. A cyclic voltammetry (CV) experiment was performed to evaluate the electrochemical stability of the two- and three-component DESQ hybrids with and without LiTFSI. Oxidation and redox peaks were observed for three imidazolium salt-based hybrids ([R-$SiO_{1.5}$]/[EMIBr]/[$(MITFSI)_2C_4O$] = 100/200/0, 100/200/1, and 100/200/1 + Li 10 wt%, Fig. S21†). The shape of the CV profile of the DESQ hybrid with 10 wt% LiTFSI remained relatively unaltered compared with those of the two- and three-component hybrids, implying that the addition of LiTFSI had no remarkable effect on the electrochemical properties. After 50 cycles, the CV peaks of the imidazolium salt-based hybrids remained unchanged compared to those for the first cycle, suggesting good cycling stability, regardless of the presence of the Li salt and cross-linker. In all cases, no additional volatile organic solvent was employed during mixing and no purification steps were necessary. Consequently, all components in the feed remained in the resulting DESQ hybrids, implying 100% atom economy, which contributes to the production of safer, greener, and cost-effective electrolytes. This sustainable approach opens a new avenue for obtaining deep eutectic-based organic–inorganic hybrids with three-dimensional structures and predetermined HBD/HBA combinations with sophisticated properties and features.

Conclusions

In summary, we reported a simple and facile preparation method of deep eutectic ion-conductive hybrids by combining hydroxyl-functionalized SQ and mono-/difunctional HBAs. Hydroxyl-functionalized SQ was first used as a polyol-type HBD to design a series of ion-conductive hybrids obtained *via* a solvent-free green process. Different ratios of SQ and mono-/difunctional HBAs were used to tune the thermal, physical, and ion-conductive properties. In this study, we proposed a novel structural strategy that allows chemical linkage of more than 50 hydroxyl groups, corresponding to the polyol-type HBD, on a single SQ nanoparticle that can interact with mono/difunctional HBAs, resulting in the formation of hydrogen bond networks. Characterization studies using DCS, TGA, viscosity, and ionic conductivity measurements verified the successful formation of DESQ hybrids with unique deep eutectics. The three-component hybrids with 1 mol% cross-linkable HBA exhibited improved thermal properties while maintaining good ionic conductivity and structural integrity. In these two- and three-component systems, a suitable HBD/HBA/cross-linkable HBA molar ratio and reaction temperature were required to achieve eutectic hybrids with the desired physical and chemical properties. DEE formation by combining HBAs and HBDs chemically linked on the SQ nanoparticle surface provides a new tool for developing deep eutectic hybrids, offering a platform for studying the ion-conductive properties on a nanoscale surface. The fabricated HBA and HBD combinations linked to the nanoparticle surface are potential building blocks for future safer, greener, and more cost-effective solid-state electrolytes.

Author contributions

Tomohito Inoue: investigation, methodology, and writing – original draft. Sota Saito: investigation. Akihiro Nishioka: vali-

dation and writing – review & editing. Hideharu Mori: conceptualization, supervision, validation, and writing – review & editing.

Data availability

The data supporting this article have been included as part of the ESI.†

Conflicts of interest

There are no conflicts to declare.

Acknowledgements

This work was financially supported by the Murata Science Foundation.

References

1 A. P. Abbott, G. Capper, D. L. Davies, R. K. Rasheed and V. Tambyrajah, *Chem. Commun.*, 2003, 70–71.
2 Q. Zhang, K. D. O. Vigier, S. Royer and F. Jerome, *Chem. Soc. Rev.*, 2012, **41**, 7108–7146.
3 E. L. Smith, A. P. Abbott and K. S. Ryder, *Chem. Rev.*, 2014, **114**, 11060–11082.
4 A. Paiva, R. Craveiro, I. Aroso, M. Martins, R. L. Reis and A. R. C. Duarte, *ACS Sustainable Chem. Eng.*, 2014, **2**, 1063–1071.
5 D. A. Alonso, A. Baeza, R. Chinchilla, G. Guillena, I. M. Pastor and D. J. Ramon, *Eur. J. Org. Chem.*, 2016, **4**, 612–632.
6 P. Liu, J.-W. Hao, L.-P. Mo and Z.-H. Zhang, *RCS Adv.*, 2015, **5**, 48675–48704.
7 L. I. N. Tome, V. Baiao, W. da Silva and C. M. A. Brett, *Appl. Mater. Today*, 2018, **10**, 30–50.
8 D. V. Wagle, H. Zhao and G. A. Baker, *Acc. Chem. Res.*, 2014, **47**, 2299–2308.
9 X. Ge, C. Gu, X. Wang and J. Tu, *J. Mater. Chem. A*, 2017, **5**, 8209–8229.
10 D. Carriazo, M. C. Serrano, M. C. Gutierrez, M. L. Ferrer and F. del Monte, *Chem. Soc. Rev.*, 2012, **41**, 4996–5014.
11 J. D. Mota-Morales, R. J. Sanchez-Leija, A. Carranza, J. A. Pojman, F. del Monte and G. Luna-Barcenas, *Prog. Polym. Sci.*, 2018, **78**, 139–153.
12 L. C. Tome and D. Mecerreyes, *J. Phys. Chem. B*, 2020, **124**, 8465–8478.
13 M. Wysokowski, R. K. Luu, S. Arevalo, E. Khare, W. Stachowiak, M. Niemczak, T. Jesionowski and M. J. Buehler, *Chem. Mater.*, 2023, **35**, 7878–7903.
14 M. H. Chakrabarti, F. S. Mjalli, I. M. AiNashef, M. A. Hashim, M. A. Hussain, L. Bahadori and C. T. J. Low, *Renewable Sustainable Energy Rev.*, 2014, **30**, 254–270.
15 Y. Hu, H. Li, X. Huang and L. Chen, *Electrochem. Commun.*, 2004, **6**, 28–32.
16 V. Lesch, A. Heuer, B. R. Rad, M. Winter and J. Smiatek, *Phys. Chem. Chem. Phys.*, 2016, **18**, 28403–28408.
17 O. E. Geiculescu, D. D. DesMarteau, S. E. Creager, O. Haik, D. Hirshberg, Y. Shilina, E. Zinigrad, M. D. Levi, D. Aurbach and I. C. Halalay, *J. Power Sources*, 2016, **307**, 519–525.
18 H. Liang, H. Li, Z. Wang, F. Wu, L. Chen and X. Huang, *J. Phys. Chem. B*, 2001, **105**, 9966–9969.
19 H. Ogawa and H. Mori, *Phys. Chem. Chem. Phys.*, 2020, **22**, 8853–8863.
20 L. Millia, V. Dall'Asta, C. Ferrara, V. Berbenni, E. Quartarone, F. M. Perna, V. Capriati and P. Mustarelli, *Solid State Ionics*, 2018, **323**, 44–48.
21 A. Boisset, S. Menne, J. Jacquemin, A. Balducci and M. Anouti, *Phys. Chem. Chem. Phys.*, 2013, **15**, 20054–20063.
22 K. Qu, X. Lu, N. Jiang, J. Wang, Z. Tao, G. He, Q. Yang and J. Qiu, *ACS Energy Lett.*, 2024, **9**, 1192–1209.
23 J. Wu, Q. Liang, X. Yu, Q.-F. Lu, L. Ma, X. Qin, G. Chen and B. Li, *Adv. Funct. Mater.*, 2021, **31**, 2011102.
24 R. K. Luu, M. Wysokowski and M. J. Buehler, *Appl. Phys. Lett.*, 2023, **122**, 234103.
25 L. N. Sim, R. Yahya and A. K. Arof, *Opt. Mater.*, 2016, **56**, 140–144.
26 K. Ajino, A. Torii, H. Ogawa and H. Mori, *Polymer*, 2020, **204**, 122803.
27 B. Joos, J. Volders, R. R. da Cruz, E. Baeten, M. Safari, M. K. Van Bael and A. T. Hardy, *Chem. Mater.*, 2020, **32**, 3783–3793.
28 M. W. Logan, S. Langevin, B. Tan, A. W. Freeman, C. Hoffman Jr., D. B. Trigg and K. Gerasopoulos, *J. Mater. Chem. A*, 2020, **8**, 8485–8495.
29 P. Jaumaux, Q. Liu, D. Zhou, X. Xu, T. Wang, Y. Wang, F. Kang, B. Li and G. Wang, *Angew. Chem., Int. Ed.*, 2020, **59**, 9134–9142.
30 B. Joos, T. Vranken, W. Marchal, M. Safari, M. K. Van Bael and A. T. Hardy, *Chem. Mater.*, 2018, **30**, 655–662.
31 Y. Chen, C. Ling, K. Long, X. Liu, P. Xiao, Y.-Z. Yu, W. Wei, X. Ji, W. Tang, G.-C. Kuang and L. Chen, *Chem. Eng. J.*, 2024, **488**, 150888.
32 Y. Tanizaki, Y. Maeda, Y. Sasaki, H. Ogawa and H. Mori, *Mater. Today Chem.*, 2021, **20**, 100455.
33 G. Yang, C. Chanthad, H. Oh, I. A. Ayhan and Q. Wang, *J. Mater. Chem. A*, 2017, **5**, 18012–18019.
34 D. Shang, J. Fu, Q. Lu, L. Chen, J. Yin, X. Dong, Y. Xu, R. Jia, S. Yuan, Y. Chen and W. Deng, *Solid State Ionics*, 2018, **319**, 247–255.
35 J. Fu, Q. Lu, D. Shang, L. Chen, Y. Jiang, Y. Xu, J. Yin, X. Dong, W. Deng and S. Yuan, *J. Mater. Sci.*, 2018, **53**, 8420–8435.
36 T. Ishii, T. Enoki, T. Mizumo, J. Ohshita and Y. Kaneko, *RCS Adv.*, 2015, **5**, 15226–15232.
37 Y. Maeda, Y. Sonta, Y. Sasaki and H. Mori, *Polymer*, 2023, **269**, 125704.
38 A. P. Abbott, J. C. Barron, K. S. Ryder and D. Wilson, *Chem. – Eur. J.*, 2007, **13**, 6495–6501.

39 B. B. Hansen, S. Spittle, B. Chen, D. Poe, Y. Zhang, J. M. Klein, A. Horton, L. Adhikari, T. Zelovich and B. W. Doherty, *Chem. Rev.*, 2021, **121**, 1232–1285.
40 H. Mori, M. G. Lanzendörfer, A. H. E. Müller and J. E. Klee, *Macromolecules*, 2004, **37**, 5228–5238.
41 H. Mori, A. H. E. Müller and J. E. Klee, *J. Am. Chem. Soc.*, 2003, **125**, 3712–3713.
42 A. P. Abbott, D. Boothby, G. Capper, D. L. Davies and R. K. Rasheed, *J. Am. Chem. Soc.*, 2004, **126**, 9142–9147.
43 Y. Zhang, M. Li, B. Qin, L. Chen, Y. Liu, X. Zhang and C. Wang, *Chem. Mater.*, 2020, **32**, 6310–6317.
44 H.-S. Jin, H.-J. Wang, Y. Zhang, Y.-J. Zuo and C.-M. Zhong, *Acta Crystallogr., Sect. E: Struct. Rep. Online*, 2007, **63**, o1880–o1881.
45 P. Fan, H. Liu, V. Marosz, N. T. Samuels, S. L. Suib, L. Sun and L. Liao, *Adv. Funct. Mater.*, 2021, **31**, 2101380.
46 A. P. Abbott, R. C. Harris and K. S. Ryder, *J. Phys. Chem. B*, 2007, **111**, 4910–4913.
47 N. Delgado-Mellado, M. Larriba, P. Navarro, V. Rigual, M. Ayuso, J. Garcia and F. Rodriguez, *J. Mol. Liq.*, 2018, **260**, 37–43.